AGU PUBLICATIONS

Geophysical Research Letters

RESEARCH LETTER
10.1002/2016GL070965

Key Points:
- The IR energy budget of the thermosphere for past 70 years has been constructed using standard solar and geomagnetic indices and SABER data
- Radiated IR power shows relatively small (< 7%) variation over five complete solar cycles, due to similar variation in solar energy input
- New indices are proposed that represent physical and measurable properties of the global thermosphere directly related to solar variability

Correspondence to:
M. G. Mlynczak,
m.g.mlynczak@nasa.gov

Citation:
Mlynczak, M. G., L. A. Hunt, J. M. Russell III, B. T. Marshall, C. J. Mertens, and R. E. Thompson (2016), The global infrared energy budget of the thermosphere from 1947 to 2016 and implications for solar variability, *Geophys. Res. Lett.*, *43*, 11,934–11,940, doi:10.1002/2016GL070965.

Received 23 AUG 2016
Accepted 3 OCT 2016
Accepted article online 6 OCT 2016
Published online 2 DEC 2016

The global infrared energy budget of the thermosphere from 1947 to 2016 and implications for solar variability

Martin G. Mlynczak[1], Linda A. Hunt[2], James M. Russell III[3], B. Thomas Marshall[4], Christopher J. Mertens[1], and R. Earl Thompson[4]

[1]NASA Langley Research Center, Hampton, Virginia, United States, [2]Science Systems and Applications Incorporated, Hampton, Virginia, United States, [3]Center for Atmospheric Sciences, Hampton University, Hampton, Virginia, United States, [4]GATS, Inc., Newport News, Virginia, United States

Abstract We present an empirical model of the global infrared energy budget of the thermosphere over the past 70 years. The $F_{10.7}$, *Ap*, and *Dst* indices are used in linear regression fits to the 14.5 year time series of radiative cooling by carbon dioxide and nitric oxide measured by the Sounding of the Atmosphere using Broadband Emission Radiometry (SABER) instrument on the TIMED satellite. Databases of these indices are used to develop the radiative cooling time series from 1947. No consistent relation between the occurrence of peak sunspot number and peak infrared cooling is found over the past six solar cycles. The total infrared energy radiated by the thermosphere, integrated over a solar cycle, is nearly constant over five complete solar cycles studied. This is a direct consequence of the geoeffective solar energy also being nearly constant over the same intervals. These results provide a new metric for assessing the terrestrial context of the long-term record of solar-related indices.

1. Introduction

A fundamental question in solar-terrestrial physics is how does the variability of the Sun influence the thermal structure, chemical composition, and energetics of the Earth's atmosphere. A common measure of solar variability is the sunspot number [*Clette et al.*, 2014]. The Sun is currently in the declining phase of solar cycle 24 (SC 24), which, as measured by sunspot number, is perhaps the weakest in the past 100 years (see Figure 1). Understanding the variability imposed on the atmosphere by the Sun is also critically important for separating natural variability from anthropogenic effects on the atmosphere, such as those associated with increasing carbon dioxide [*Yue et al.*, 2015].

For the past 14.5 years, for half of SC 23 and all of SC 24 to date, the SABER instrument [*Russell et al.*, 1999] on the NASA TIMED satellite has been observing the thermal structure, chemical composition, and energy balance of the terrestrial atmosphere between 15 and 250 km [*Mlynczak*, 1997]. In particular, SABER has provided unique measurements on the infrared energy budget of the thermosphere above 100 km. Energy from the Sun in the form of electromagnetic radiation and solar wind particles heats the thermosphere. The thermosphere cools to space primarily by infrared energy radiated by carbon dioxide (CO_2) at 15 μm and by nitric oxide (NO) at 5.3 μm. These measurements have been used in a variety of ways to study the energetics of the thermosphere, e.g., *Mlynczak et al.* [2003, 2014], *Knipp et al.* [2013], and *Verkhoglyadova et al.* [2016].

In a first step at examining infrared cooling over several solar cycles, *Mlynczak et al.* [2015] developed the Thermosphere Climate Index (TCI). The TCI is a multiple linear regression fit of the SABER-observed global thermospheric cooling by NO using the $F_{10.7}$, *Ap*, and *Dst* solar and geomagnetic indices, which are extant from the year 1947. *Mlynczak et al.* [2015] examined the relative roles of solar and geomagnetic processes in generating the energy that drives radiative cooling by NO. They found that while solar ultraviolet irradiance is generally dominant, geomagnetic processes become relatively more important during solar minimum.

In this paper we build upon *Mlynczak et al.* [2015] to represent the time series of global radiative cooling of the thermosphere by CO_2 with a multiple linear regression involving the same solar and geomagnetic indices. This enables the derivation of the infrared energy budget of the thermosphere (CO_2 and NO cooling) from 1947 to the present day, a time span covering 70 years and five complete solar cycles. The empirically derived time series enables an examination of the variability of infrared cooling due to the variability of input energy from the Sun over the same time. The derived time series also enables us to examine the relationship of the occurrence of sunspot maximum to the maximum in total infrared cooling. A goal of this work is to

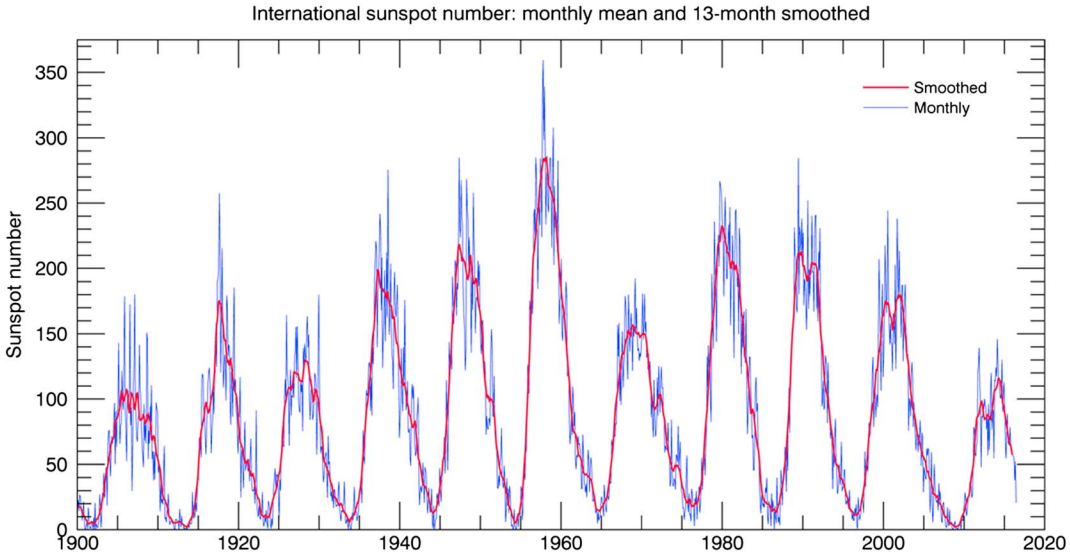

Figure 1. Plot of the sunspot number from 1900 to the present day. Monthly mean data (blue curve) and 13-month smoothed data (red curve) are shown.

develop new, physically meaningful metrics for assessing the effects of the variability of solar energy output on the Earth's thermosphere.

In the next section we review the SABER radiative infrared cooling data and the time series of solar and geomagnetic indices. Results and analyses are presented in section 3. The paper concludes with a summary in section 4.

2. Data and Methodology

The time series of SABER thermospheric infrared radiative cooling data has been previously described in detail [*Mlynczak et al.*, 2014, and references therein]. The time series are of the total radiated power (W) by NO and by CO_2 on a daily basis and integrated over the Earth. The SABER instrument measures infrared

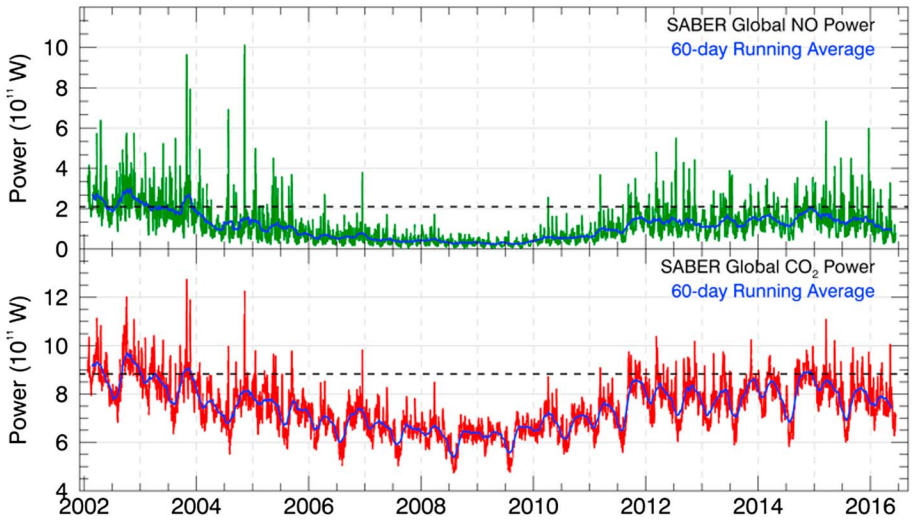

Figure 2. The SABER time series of daily global power radiated from the thermosphere (above 100 km) by (top) nitric oxide (NO, green curve) and (bottom) carbon dioxide (CO_2, red curve). The blue curve is the 60 day running mean of each time series. The dashed black lines mark the occurrence of peak power in SC 24 (December 2014) and 11 years prior in SC 23 (December 2003).

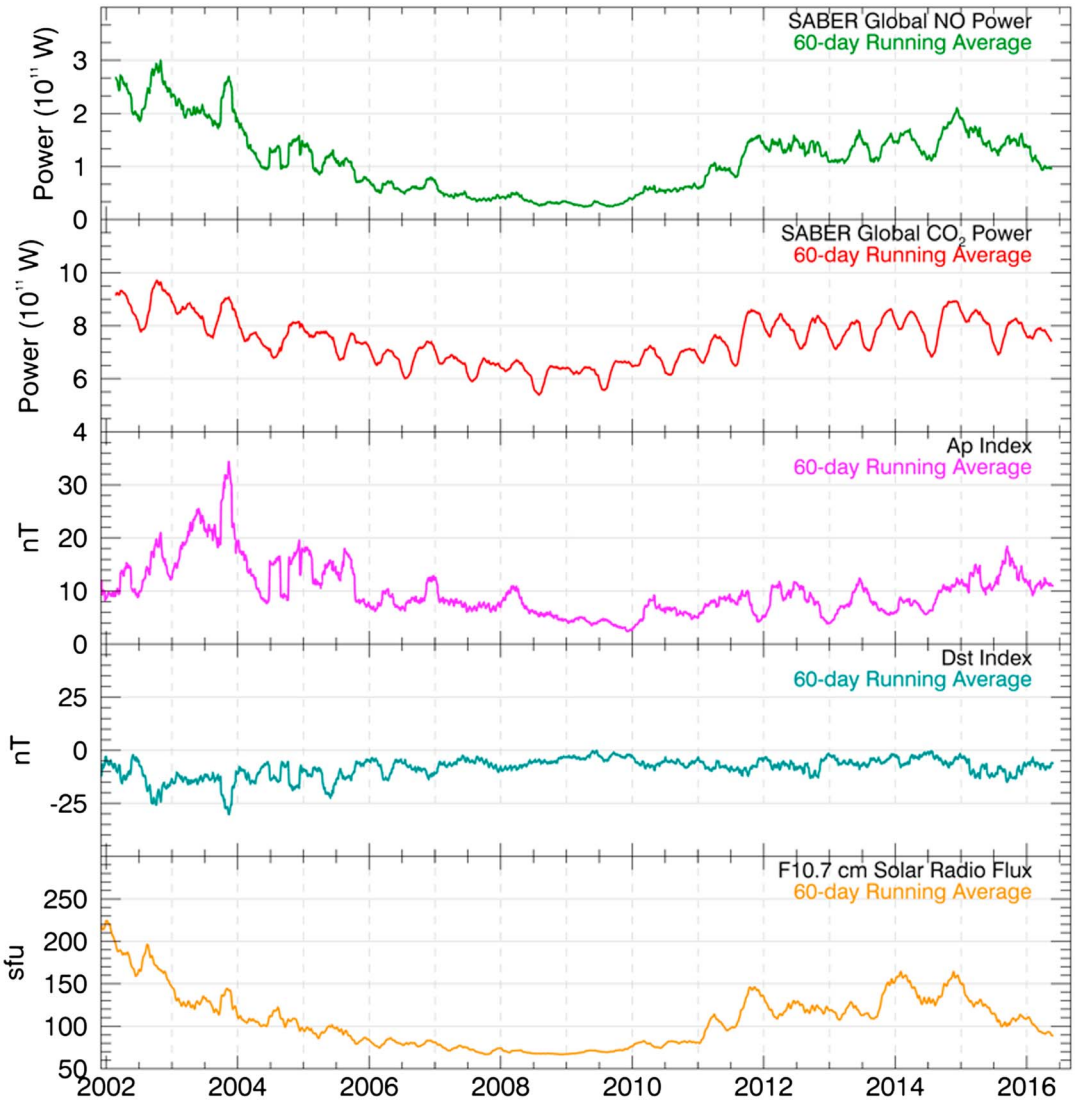

Figure 3. (top to bottom) The 60 day running mean of the SABER daily NO power, the daily CO_2 power, the daily average *Ap* index, the daily average *Dst* index, and the daily $F_{10.7}$ cm solar radio flux. Strong visual correlations are evident between the infrared power measurements and the solar and geomagnetic indices.

radiance profiles of the Earth's limb at 5.3 μm (NO) and 15 μm (CO_2). These radiance ($W/m^2/sr$) profiles (1500 per day) are used to generate vertical profiles of infrared radiative cooling rates (W/m^3) [*Mlynczak et al.*, 2010]. These profiles are then integrated vertically (over the range 100 to 250 km) to generate fluxes (W/m^2) of radiation that exit the thermosphere. The fluxes are then integrated with respect to area over the entire Earth to yield the total power (W) radiated by NO and CO_2. Their sum provides a measure of the total infrared power exiting the thermosphere.

Figure 2 shows the SABER time series of the daily global radiated power by NO (green) and by CO_2 (red) from 22 January 2002 through 15 July 2016, nearly 5300 days. The blue curve shows the 60 day running average of each of the daily cooling time series. A 60 day mean is chosen because the TIMED satellite samples all local times in 60 days. Perhaps the most evident features are the large "spikes" in the data—these are not measurement noise, but rather, they are due to real geophysical variability of space weather. The large events evident in October 2003 and November 2004 in both NO and CO_2 are major geomagnetic storm events, the former being the celebrated "Halloween storms" of 2003. The infrared emission increases dramatically as the thermosphere is heated due to particle precipitation and acts as a "natural thermostat," to return the temperature to its prestorm conditions [*Mlynczak et al.*, 2003].

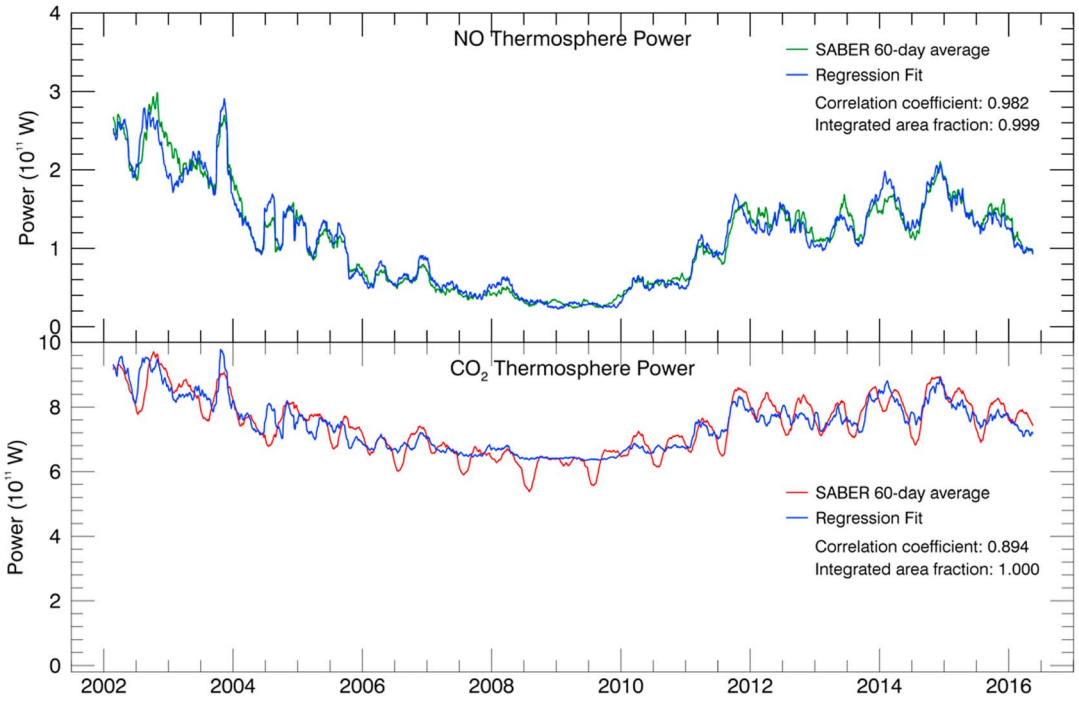

Figure 4. Plot of the (top) NO 60 day running mean power and the multiple linear regression (MLR) fit using the $F_{10.7}$, *Ap*, and *Dst* indices and of the (bottom) CO_2 60 day running mean and the corresponding MLR fit. The correlation coefficients for the fits are high (0.982, NO; 0.894, CO_2) and the area under the observed and fit curves is identical in both cases.

The CO_2 power data also exhibit annual and semiannual cycles [*Mlynczak et al*., 2008] that are visually evident in the 60 day mean power. These cycles are due to processes that originate in the atmosphere [*Emmert*, 2015] and are not directly solar driven. And finally, clearly visible in Figure 2 is the 11 year solar cycle, evidenced by the larger NO and CO_2 cooling values in 2002, followed by the minimum values in 2008–2009, and another cooling maximum in late 2014. The dashed line across each of the two figures is set at the 60 day average cooling peak in NO and CO_2 reached in December 2014. Extending back, it is evident that similar levels of 60 day radiative power were last reached 11 years prior in late 2003. Furthermore, going back to the beginning of the mission, the 60 day power levels were not much larger than the peak power reached in 2014, despite SC 24 being considered a much weaker solar cycle than its predecessor. Thus, this result raises the question: how different from one another are solar cycles in terms of infrared radiative power?

To answer this question, we follow *Mlynczak et al*. [2015] and show in Figure 3 the 60 day running average time series of NO radiative power, CO_2 radiative power, the *Ap* index, the *Dst* index, and the $F_{10.7}$ cm solar radio flux. There are clear visual correlations between both radiative power time series and the solar and geomagnetic index time series. Shown in Figure 4 are the multiple linear regression fits of the NO (top) and CO_2 (bottom) power time series to the $F_{10.7}$, *Ap*, and *Dst* indices. The NO power time series extends that of *Mlynczak et al*. [2015] by more than a year. The correlation coefficient for the fit to the NO power is 0.982 and the ratio of the integrated area of the fit curve to the integrated NO time series is 0.999. This result demonstrates the fit preserves the time-integrated power, which is critical for the upcoming comparison of total energy radiated over different solar cycles.

Figure 4 (bottom) shows the multiple linear regression fit to the SABER time series of 60 day running average CO_2 power. The correlation coefficient of the fit is 0.894, while the ratio of the fit to observed integrated area is 1.0. The correlation coefficient is lower than in the case for NO because we do not fit an annual or semiannual cycle to the SABER data because, as noted above, these features originate within the atmosphere. However, as with NO, the integrated area is preserved with the fit, which is the critical requirement for developing an accurate infrared energy budget time series from 1947.

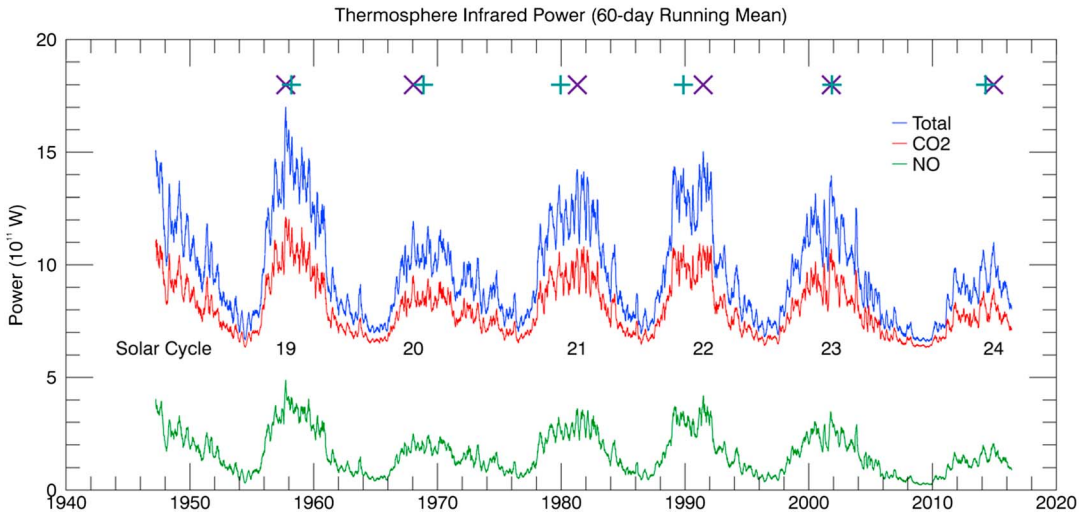

Figure 5. The empirically derived infrared energy budget of the thermosphere from 1947 to 2016. The total radiated power from NO (green), CO_2 (red), and their sum (blue) are shown. The solar cycle number is shown in the middle of the plot. The occurrence of sunspot maximum (plus) and the infrared cooling maximum (cross) is shown.

3. Results

The coefficients for the least squares fits shown in Figures 3 and 4 are used with existing databases of the $F_{10.7}$, *Ap*, and *Dst* indices to construct the infrared power emitted by NO and CO_2 back to 1947, which date is the beginning of the $F_{10.7}$ time series. Figure 5 shows the empirically derived NO and CO_2 power time series (green and red curves, respectively), while their sum is shown in the blue curve. The solar cycle number (18 through 24) is also indicated. The time series covers five complete solar cycles (19 through 23). SABER continues to take data as the Sun is approaching its next minimum. As of this writing, SABER is approved to operate through September 2017, and in early 2017 NASA will decide whether to extend its operations for another 2 years.

To examine the difference in radiated energy for each complete solar cycle, we integrate the power in each of the three curves, from one minimum in total power to the next, over the five complete cycles shown. The results of this integration are given in Table 1, along with the number of days considered in each integration. There are columns for integrated power for NO, for CO_2, and for their sum, covering each of the five complete solar cycles. The sixth column in Table 1 shows the integration of the $F_{10.7}$ index, and the seventh column in Table 1 is the integration of the *Ap* index. Upon examination of the integrated total power in Table 1, we see that the variation of total infrared power from one solar cycle to the next is quite small, certainly smaller than might have been expected from a visual examination of the solar variability implied by the sunspot number time series in Figure 1. We find the standard deviation about the mean of the global infrared power radiated by the thermosphere to be less than 7% over the five complete solar cycles considered. The larger power

Table 1. The Sunspot Cycle Number, Cycle Length (Days), Integrated NO Power (W), Integrated CO_2 Power (W), Total (Sum Of NO And CO_2) Power (W), Integrated $F_{10.7}$ Solar Flux (1 sfu = 10^{-22} J s^{-1} m^{-2} Hz^{-1}), and Integrated *Ap* (nT) for Each of the Five Complete Solar Cycles[a]

Sunspot Cycle	Cycle Length (Days)	Sum NO Power (10^{14} W)	Sum CO_2 Power (10^{15} W)	Total Power (10^{15} W)	Sum $F_{10.7}$ (10^5 sfu)	Sum *Ap* (10^4 nT)
19	3692	7.48	3.16	3.91	5.30	5.97
20	4242	5.88	3.28	3.87	4.81	5.47
21	3623	6.86	3.03	3.72	4.97	5.67
22	3629	6.69	3.02	3.69	4.85	5.66
23	4761	6.55	3.69	4.35	5.54	5.58
	Mean	6.69	3.23	3.90	5.09	5.67
	Std. Dev.	8.6%	8.5%	6.7%	6.1%	3.3%

[a]The mean and standard deviation of the various properties are given in the bottom two rows.

value for solar cycle 23 is an outlier; this is the longest of the five cycles examined and also had a very deep minimum in 2008–2009 when record low thermospheric densities were observed [*Emmert et al*., 2010]. Excluding cycle 23, the standard deviation of integrated total power is 2.9%.

Figure 5 also shows the occurrence of the infrared radiative cooling maximum (cross) and the occurrence of the sunspot maximum (plus). For the six maxima pairs indicated in Figure 5, the infrared cooling maximum occurs after the sunspot maximum three times and before the sunspot maximum twice. They are coincident only once, during solar cycle 23. There is no consistent relationship between the temporal occurrences of these two events in the six solar cycles examined here.

The lack of variation in the infrared radiative cooling from the thermosphere has significant implications for the variability of the energy input to the thermosphere over the same time periods. Specifically, infrared radiation, integrated over time, is a direct measure of the energy input over the same time. The result presented here, of relatively small variations in infrared radiation, when integrated from one minimum in total radiation to the next, implies that the input energy to the thermosphere also has correspondingly small variations over the same time. This conclusion follows from fundamental physics and from the linear relationships formed to relate total infrared cooling to the solar and geomagnetic indices, the latter of which also contains information on solar variability. Indeed, we find that the $F_{10.7}$ and *Ap* indices, integrated over a solar cycle, exhibit very small variations from one solar cycle to the next. This result is shown in the two rightmost columns of Table 1. The standard deviation of $F_{10.7}$ about the mean is 6.1% over the five solar cycles studied, and the standard deviation of *Ap* is 3.3%. Thus, the correct interpretation of the results presented here is that the relative invariance of the empirically derived thermospheric infrared cooling is a direct result of the relative invariance of the geoeffective solar energy input to the thermosphere from one solar cycle to the next. The relatively small invariance in total solar output from one cycle to the next has been previously anticipated. *Kane* [2008] and *Dikpati et al.* [2010] have shown the length of a solar cycle is anticorrelated with the following cycle's strength, which suggests uniform area under the cycles' activity curves.

4. Summary

The daily global infrared power radiated from the thermosphere above 100 km by CO_2 and NO has been derived back to 1947 using a 14-plus year data set of infrared radiated power observed by the SABER instrument on the TIMED satellite. These empirical relationships are developed through multiple linear regression fits to the observed power with the $F_{10.7}$, *Ap*, and *Dst* indices. The database of these indices goes back to 1947, enabling a time series that covers five complete solar cycles (19 through 23). Integration of the total (CO_2 plus NO) power from one minimum in total power to the next reveals that, over each complete solar cycle, the amount of infrared energy radiated by the thermosphere is relatively constant. This result implies that the amount of energy input from the Sun (ultraviolet photons and particle precipitation associated with geomagnetic events) is also relatively constant over the same time period. This implication is borne out by the integration of the $F_{10.7}$ and *Ap* indices over the same time periods, which shows variation similar to that in total radiated infrared power. Thus, it is the relatively small variations in geoeffective solar energy input to the thermosphere (over a solar cycle) that is responsible for the derived small variations in infrared cooling.

In closing, in an extension of *Mlynczak et al*. [2015], we suggest that the total infrared power (the blue curve in Figure 5) should be considered as a new index for describing the state of the thermosphere and the effects of solar and geomagnetic activity on it. The least squares equations for the NO power, the CO_2 power, and the total power (units of 10^{11} W) are given by

$$CO_2 = 4.720 + 2.127 \times 10^{-2} \times F_{10.7} + 4.043 \times 10^{-2} \times Ap - 8.704 \times 10^{-3} \times Dst \quad (1)$$

$$NO = -1.024 + 1.562 \times 10^{-2} \times F_{10.7} + 4.637 \times 10^{-2} \times Ap - 4.013 \times 10^{-3} \times Dst \quad (2)$$

$$Total = 3.696 + 3.689 \times 10^{-2} \times F_{10.7} + 8.680 \times 10^{-2} \times Ap - 1.272 \times 10^{-2} \times Dst \quad (3)$$

The units used are solar flux units (sfu) for $F_{10.7}$ ($1\ sfu = 10^{-22}\ J\ s^{-1}\ m^{-2}\ Hz^{-1}$) and nanoteslas for *Ap* and *Dst*. The $F_{10.7}$, *Ap*, and *Dst* indices used in equations 1–3 are centered, 60 day running means. As suggested by *Mlynczak et al*. [2015], these indices are climate-related indices, as they provide an estimate of the total energy output from the thermosphere, and based on the results of this paper, they also give an estimate

of the total energy input to the thermosphere. The indices represent a fundamental physical and measurable quantity of the global atmosphere that is ultimately dependent on the thermal structure and composition of the atmosphere. The indices can be updated regularly and serve as direct monitors of the state of the thermosphere in response to ongoing solar and geomagnetic variability, effectively providing a terrestrial context to the long-term record of solar-related indices. A future paper will discuss this in more detail and will also recommend adjectival descriptions for the numerical values based on their observed distribution over the 70 years of the time series.

Acknowledgments

The *Ap* and $F_{10.7}$ data are from the geomagnetic and solar databases at the NOAA Space Weather Prediction Center. The *Dst* data are from the University of Oulu, Finland, http://dcx.oulu.fi. The daily sunspot data are from the World Data Center for Sunspot Index and Long-term Solar Observations at Royal Observatory of Belgium, Brussels. The NO and CO_2 power data are available from the first author of this article. The authors acknowledge support from the NASA TIMED project.

References

Clette, F., L. Svalgaard, J. M. Vaquero, and E. W. Cliver (2014), Revisiting the sunspot number: A 400-year perspective on the solar cycle, *Space Sci. Rev.*, *185*, 35–103, doi:10.1007/s11214-014-0074-2.

Dikpati, M., P. A. Gilman, and R. P. Kane (2010), Length of a minimum as predictor of next solar cycle's strength, *Geophys. Res. Lett.*, *37*, L06104, doi:10.1029/2009GL042280.

Emmert, J. T. (2015), Thermospheric mass density: A review, *Adv. Space Res.*, *56*, 773–824, doi:10.1016/j.asr.2015.05.038.

Emmert, J. T., J. L. Lean, and J. M. Picone (2010), Record-low thermospheric density during the 2008 solar minimum, *Geophys. Res. Lett.*, *37*, L12102, doi:10.1029/2010GL043671.

Kane, R. P. (2008), Prediction of solar cycle maximum using solar cycle lengths, *Sol. Phys.*, *248*, 203–209, doi:10.1007/s11207-008-9125-8.

Knipp, D., L. Kilcommons, L. Hunt, M. Mlynczak, V. Pilipenko, B. Bowman, Y. Deng, and K. Drake (2013), Thermospheric damping response to sheath-enhanced geospace storms, *Geophys. Res. Lett.*, *40*, 1263–1267, doi:10.1002/grl.50197.

Mlynczak, M., et al. (2003), The natural thermostat of nitric oxide emission at 5.3 μm in the thermosphere observed during the solar storms of April 2002, *Geophys. Res. Lett.*, *30*(21), 2100, doi:10.1029/2003GL017693.

Mlynczak, M. G. (1997), Energetics of the mesosphere and lower thermosphere and the SABER experiment, *Adv. Space Res.*, *20*(6), 1177–1183, doi:10.1016/S0273-1177(97)00769-2.

Mlynczak, M. G., F. Javier Martin-Torres, C. J. Mertens, B. T. Marshall, R. E. Thompson, J. U. Kozyra, E. E. Remsberg, L. L. Gordley, J. M. Russell III, and T. Woods (2008), Solar-terrestrial coupling evidenced by periodic behavior in geomagnetic indexes and the infrared energy budget of the thermosphere, *Geophys. Res. Lett.*, *35,* L05805, doi:10.1029/2007GL032620.

Mlynczak, M. G., et al. (2010), Observations of infrared radiative cooling in the thermosphere on daily to multiyear timescales from the TIMED/SABER instrument, *J. Geophys. Res.*, *115*, A03309, doi:10.1029/2009JA014713.

Mlynczak, M. G., M. G. Mlynczak, L. A. Hunt, C. J. Mertens, B. T. Marshall, J. M. Russell III, T. Woods, R. E. Thompson, and L. L. Gordley (2014), Influence of solar variability on the infrared radiative cooling of the thermosphere from 2002 to 2014, *Geophys. Res. Lett.*, *41*, 2508–2513, doi:10.1002/2014GL059556.

Mlynczak, M. G., L. A. Hunt, B. T. Marshall, J. M. Russell III, C. J. Mertens, R. E. Thompson, and L. L. Gordley (2015), A combined solar and geomagnetic index for thermospheric climate, *Geophys. Res. Lett.*, *42*, 3677–3682, doi:10.1002/2015GL064038.

Russell, J. M., M. G. Mlynczak, L. L. Gordley, J. Tansock, and R. Esplin (1999), An overview of the SABER experiment and preliminary calibration results, in *Proceedings of the 44th Annual Meeting, Denver, Colorado, July 18–23*, vol. 3756, pp. 277–288, SPIE, Bellingham, Wash.

Verkhoglyadova, O. P., B. T. Tsurutani, A. J. Mannucci, M. G. Mlynczak, L. A. Hunt, L. J. Paxton, and A. Komjathy (2016), Solar wind driving of ionosphere-thermosphere responses in three storms near St. Patrick's Day in 2012, 2013 and 2015, *J. Geophys. Res. Space Physics*, *121*, doi:10.1002/2016JA022883.

Yue, J., J. Russell III, Y. Jian, L. Rezac, R. Garcia, M. López-Puertas, and M. G. Mlynczak (2015), Increasing carbon dioxide concentration in the upper atmosphere observed by SABER, *Geophys. Res. Lett.*, *42*, 7194–7199, doi:10.1002/2015GL064696.